Yun Xu
Department of Materials Science
and Engineering,
Clemson University,
Clemson, SC 29634
e-mail: yxu4@g.clemson.edu

Mingyang Zhao
Department of Materials Science
and Engineering,
Clemson University,
Clemson, SC 29634
e-mail: mingyaz@g.clemson.edu

Syed Khalid
Photon Science Directorate,
Brookhaven National Laboratory,
Upton, NY 11973
e-mail: Khalid@bnl.gov

Hongmei Luo
Department of Chemical &
Materials Engineering,
New Mexico State University,
Las Cruces, NM 88003
e-mail: hluo@nmsu.edu

Kyle S. Brinkman[1]
Department of Materials Science
and Engineering,
Clemson University,
Clemson, SC 29634
e-mail: ksbrink@clemson.edu

Self-Substitution and the Temperature Effects on the Electrochemical Performance in the High Voltage Cathode System $LiMn_{1.5+x}Ni_{0.5-x}O_4$ ($x = 0.1$)

The high voltage cathode material, $LiMn_{1.6}Ni_{0.4}O_4$, was prepared by a polymer-assisted method. The novelty of this work is the substitution of Ni with Mn, which already exists in the crystal structure instead of other isovalent metal ion dopants which would result in capacity loss. The electrochemical performance testing including stability and rate capability was evaluated. The temperature was found to impose a change on the valence and structure of the cathode materials. Specifically, manganese tends to be reduced at a high temperature of 800 °C and leads to structural changes. The manganese substituted $LiMn_{1.5}Ni_{0.5}O_4$ (LMN) has proved to be a good candidate material for Li-ion battery cathodes displaying good rate capability and capacity retention. The cathode materials processed at 550 °C showed a stable performance with negligible capacity loss for 400 cycles. [DOI: 10.1115/1.4036386]

Introduction

To achieve extended driving distances and lower costs for electric vehicles, extensive efforts have been devoted to finding the next generation of cathode materials for Li-ion batteries. Due to the redox pair of Ni^{2+}/Ni^{4+}, spinel structured oxides like $LiMn_{1.5}Ni_{0.5}O_4$ (LMN) which has a high voltage of 4.75 V versus Li^+/Li is an appealing choice for cathodes in next generation of Li-ion batteries. However, an obstacle for the commercialization of high voltage $LiMn_{1.5}Ni_{0.5}O_4$ is the electrolyte decomposition occurring at the electrode/electrolyte interface due to an overlap of the electrolyte operation window and the operational voltage window of the electrode. A solid electrolyte interface (SEI) is known to form at the potential where nickel becomes electroactive. This results in degradation as evidenced by the reduction in capacity of the cells. It has been reported in literature that partial substitutions of Mn or Ni by other transition metal ions such as Cr, Fe, Co, Zn, Nb, and Ga can stabilize a disordered lattice [1–4] by suppressing the formation of a rocksalt impurity phase resulting in a stable electrode electrolyte interface [5]. Despite numerous reports on the influence of various cations on the electrochemical performance of LMN, there have been limited reports to date on the partial substitution of Ni by Mn [6,7]. However, Mn doping has a significant advantage over other dopants due to its high electrochemical activity.

On the other hand, carbon coating has been reported to help both electronic conductivity and form solid electrolyte interphase by accelerating surface side reaction [8,9]. In this study, we report a polymer-assisted synthesis method to prepare a carbon-coated manganese-doped cathode $LiMn_{1.6}Ni_{0.4}O_4$. Both the carbon coating and doping were achieved by a simple one-step synthesis method.

Experimental

$LiMn_{1.6}Ni_{0.4}O_4$ powders were prepared by a polymer-assisted method. Polyethylenimine (PEI) (50 wt %) and ethylenediaminetetraacetic acid (EDTA) were used to form a complex with metal ions. Lithium nitrate ($LiNO_3$), manganese acetate tetrahydrate $Mn(CH_3COO)_2 \cdot 4H_2O$, and Nickel acetate tetrahydrate $Ni(OCOCH_3)_2 \cdot 4H_2O$ were used as metal precursors. Metal additions of 0.158 g of lithium nitrate ($LiNO_3$), 0.784 g of manganese acetate tetrahydrate, and 0.198 g of nickel acetate tetrahydrate were used. The solution was prepared in two steps: (i) 1.84 g of PEI and 0.92 g of EDTA were dissolved in 10 ml of water followed by (ii) the addition of metal precursors with a stoichiometric ratio of 1:1.

The solutions of mixed metal ions were subsequently transferred to a crucible and dried in the furnace (Lindberg) at 150 °C for 8 h in order to evaporate water. The dried products were held at 400 °C for 4 h to burn off carbon followed by heat treatment at 550 °C and 800 °C for 4 h in order to achieve the targeted crystalline phase. The sample names referred to in the remainder of the text are LMN(500) and LMN(800), respectively. The heating ramp rate for all the steps was 1 °C/min. The crystal chemistry of the samples was characterized by X-ray diffraction with Cu Kα radiation ($\lambda = 0.154$ nm). The morphology was characterized by scanning electron microscope (SEM) (Hitachi). X-ray absorption

---

[1]Corresponding author.

spectroscopy was collected at Stanford Synchrotron Radiation Lightsources on beamline 2-2. The Mn K-edge near edge spectra was collected at room temperature. Data were collected in the transmission mode using N_2 filled ion chambers. The X-ray energy of the peak was calibrated by Mn foil as reference standard. Mn K-edge spectra were collected using 1 eV in the pre-edge (6339–6539 eV) and 0.35 eV steps (6539–6569 eV) in the near edge region. Electrochemical testing was carried out in CR2032 cells with lithium metal as counter electrode. Cathode slurries were prepared by dispersing the active material, super p conductive carbon, and polyvinylidene difluoride (PVDF) with a weight ratio of 70:20:10 in N-methyl pyrrolidone (NMP) solvent. This slurry was then cast onto an aluminum foil and dried under vacuum at 80 °C for 12 h. The cells were then assembled with Celgard separators (MTI Corporation, Richmond, CA) and an electrolyte of 1 M LiPF$_6$ salt dissolved in a 1:1 volume ratio of ethylene carbonate (EC)/dimethyl carbonate (DMC). All the electrolyte components were purchased from MTI Corporation. The mass loading for the cathode materials is between 1 and 2 mg; anode materials (in the full cell tests) are also 1–2 mg considering the capacity match. The capacity was calculated based on the mass loading of cathode materials.

Results and Discussion

Figure 1(a) shows the XRD patterns of the synthesized cathodes. All the samples displayed similar XRD patterns with the LiMn$_{1.5}$Ni$_{0.5}$O$_4$ reference. The peak at $2\theta = 18.9$ deg exhibited a left shift for LMN(800), indicating a larger lattice distance.
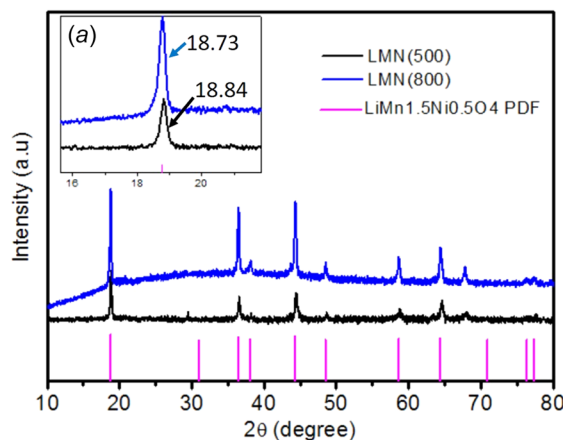
The larger lattice distance could be the result of additional Mn^{3+} content in the crystal. It is known that high-temperature annealing leads to a loss of oxygen and increases Mn^{3+} content [10]. Figure 1(b) reveals the SEM determined microstructure and morphology of the synthesized samples which were similar to previous studies of LiMn$_2$O$_4$ cathodes with particles sizes on the order of 100 nm [11]. In our previous work of LiMn$_2$O$_4$ nanoparticles prepared by the same method, a carbon layer was also observable on the surface of nanoparticles. This thin carbon layer is a residue from the burning of polymers during high-temperature annealing [11].

Cyclic voltammograms for the cathode materials were performed from 3.5 V to 5 V at a slow scan rate of 0.2 mV/s. As shown in Fig. 2(a), the voltammograms of LMN(550) and LMN(800) reveal two separate redox peaks corresponding to the Ni^{2+}/Ni^{3+} and Ni^{3+}/Ni^{4+} at 4.74 V and 4.81 V, respectively [12]. A slight bump in the signal at 4.0 V appears for the sample LMN(800), which indicates that more manganese becomes electrochemically active (more Mn^{3+} ions present) at higher processing temperatures. Similar electrochemical behavior is expected in the charge and discharge profiles. The charge and discharge mechanism can be expressed in the following equation:

$$LiMn_{1.4}^{4+}Mn_{0.2}^{3+}Ni_{0.4}^{4+}O_4 = Mn_{1.6}^{4+}Ni_{0.4}^{4+}O_4 + Li^+ + e^-$$
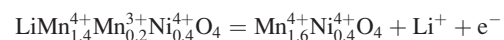
For LMN(550), a tiny plateau at ~4.0 V was observed for the redox reaction of Mn^{3+}/Mn^{4+}, while a large plateau appeared for LMN(800), which contributed approximately 30% of the
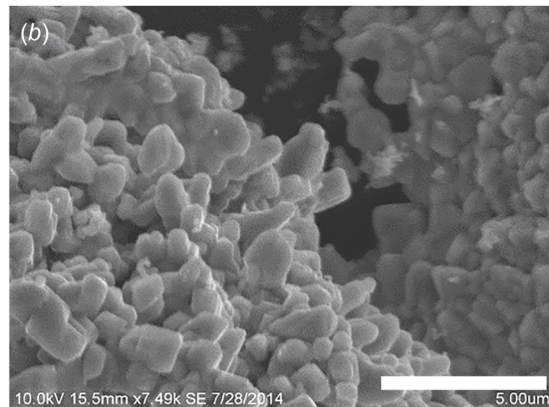

Fig. 1 (a) XRD patterns of LMN(550) and LMN(800) and (b) SEM image of synthesized particles LMN(550) sample
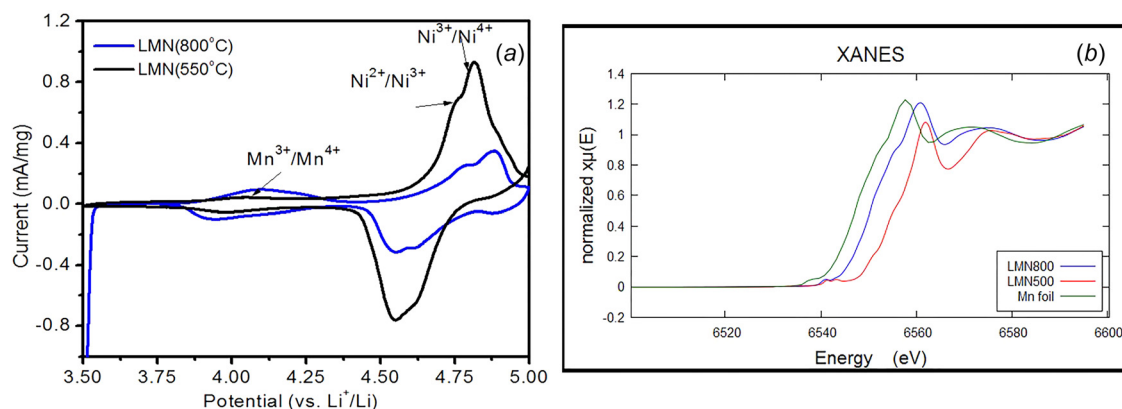

Fig. 2 (a) Cyclic voltammograms of LMN(550) and LMN(800) scanned from 3.5 V to 5 V and (b) XANES of LMN(550), LMN(800), and Mn foil
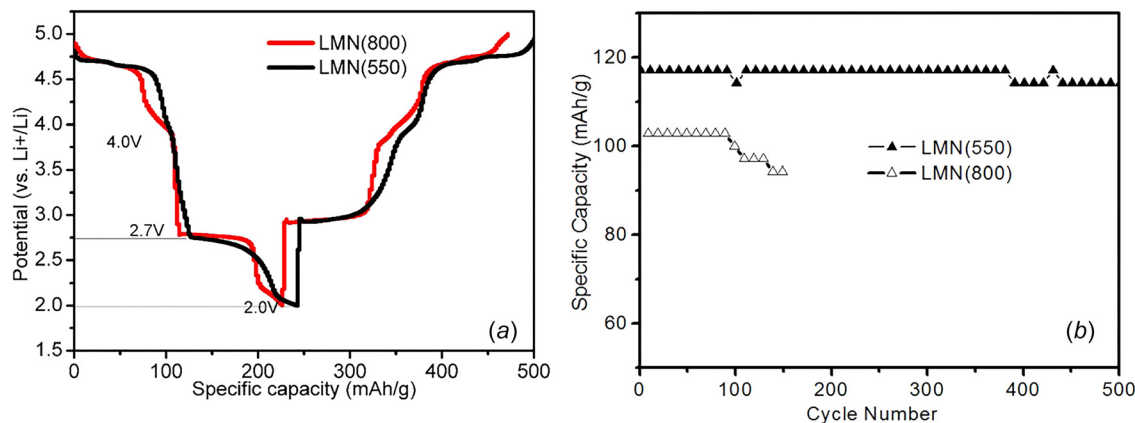
Fig. 3 (*a*) Charge and discharge profile from 1.75 V to 5 V and (*b*) cycle performance of LMN(550) and LMN(800) at 4 C

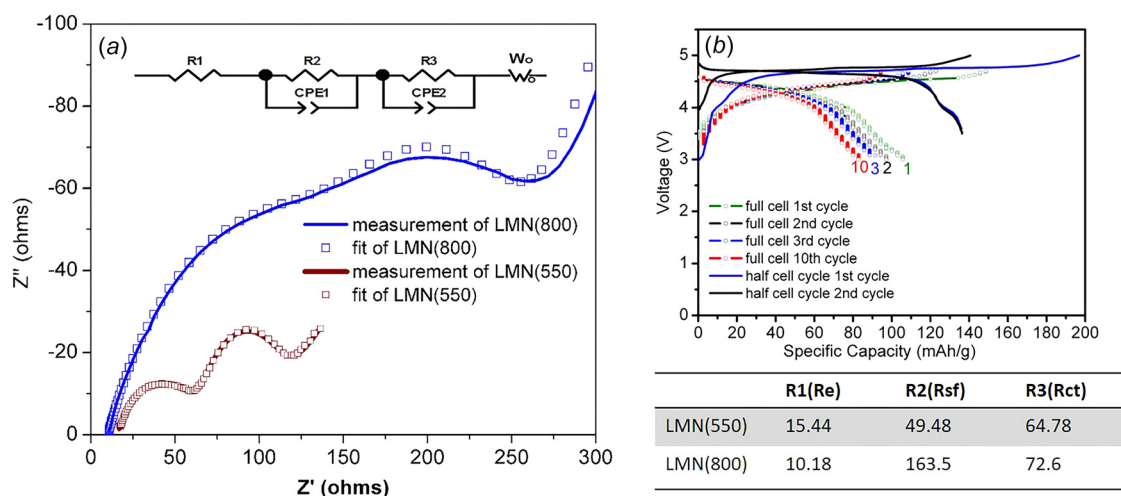|	R1(Re)	R2(Rsf)	R3(Rct)
LMN(550)	15.44	49.48	64.78
LMN(800)	10.18	163.5	72.6

Fig. 4 (*a*) Impedance spectra and the fitting result of two LMN prepared at different temperatures, inset is the equivalent circuit used to fit impedance spectra. With fitting parameters listed in the bottom table. (*b*) Charge and discharge profiles of full cell and half-cell.

discharge capacity. As pointed out earlier, the increase in Mn^{3+} at high temperature could be the reason for the increase of contribution from manganese in sample LMN(800) [10]. The presence of reduced Mn^{3+} in LMN(800) was confirmed by X-ray absorption near edge structure (XANES) experiments. Figure 2(*b*) displays the X-ray absorption spectra in the near edge range of Mn absorption edge. A sharp and intense peak was observed for both samples corresponding to $1 s \rightarrow 4 p$ transition. A comparison of sample spectra and pure metallic manganese foil indicates that the sample prepared at 800 °C was reduced to a larger extent than samples prepared at 550 °C as indicated by a shift to left in the peak.

In the $LiMn_{1.5}Ni_{0.5}O_4$ crystal structure, if all of the available Ni^{2+} ions are fully coordinated by 6 Mn^{4+} nearest-neighbors in the lattice, this would result in a space group of primitive simple cubic $P4_332$ [13]. If the Ni^{2+} and Mn^{4+} are distributed randomly among the 16 d octahedral sites, the structure belongs to a space group of face-centered-Fd_3m [14].

The degree of ordering can be determined from electrochemical characterization. The voltage profiles are shown in Fig. 3(*a*). During discharge below 3 V, there were two plateaus observed at 2.7 V and 2 V, respectively, which represent insertion of lithium ions into 16 c octahedral sites of the spinel structure. The ratio between plateau length at 2.7 V and 2 V is related to the degree of ordering [15]. A higher ratio means a higher degree of order.

Comparing the discharge profiles of the two samples, it is found that LMN(800) showed a smaller ratio, suggesting that LMN(800) is more disordered than LMN(550).

Recently, there has been some controversy as to whether ordered or disordered structures exhibit better performance [14,16]. Most reports showed that disordered structure delivers better electrochemical performance. In this work, a cycle performance test was conducted to examine the impact of structural order on cathode performance with the results displayed in Fig. 3(*b*). Galvanostatic charge and discharge were performed at a rate of 4 C. While LMN(550) displayed steady performance, LMN(800) began to severely degrade after 100 cycles. In addition to potential effects arising from the octahedral ordering, other possible degradation mechanisms are Jahn–Teller distortion originating from the excessive Mn^{3+} in LMN(800) [17].

Impedance spectra were collected for these two samples to evaluate the electrochemical performance with the Nyquist plots displayed in Fig. 4(*a*). The impedance spectra were simulated with an equivalent circuit as shown in the inset of Fig. 4(*a*). The resistance, R1(Re), represents the uncompensated ohmic resistance from electrolyte. The first parallel of resistance and constant phase element (CPE), R2(Rsf)-CPE1, represents that lithium migration occurs across the surface film. The second parallel of resistance and CPE, R3(Rct)-CPE2, represents charge-transfer resistance. The Warburg impedance, Wo, describes the solid-state

diffusion. The fitted parameters are summarized and displayed in the table on the bottom right of Fig. 4. A review of the data indicates that the LMN(550) sample showed a lower surface film resistance and charge-transfer resistance as compared to LMN(800). A possible reason for this low impedances is the presence of a thicker SEI in the LMN(800) as compared to LMN(550) sample due to carbon loss.

LMN(550) was also evaluated in the full cell with conductive graphite as the anode. The full cell was assembled similar to the half-cell, with the exception of graphite on copper foil employed as the lithium electrode. The voltage profile of the full cell is displayed in Fig. 4(b). The cell was charged and discharged in a voltage range of 3–4.7 V. The columbic efficiency and gradual capacity loss are due to SEI formation on the graphite anode surface. In the half-cell measurements, the capacity loss was negligible for the second cycle because of the protective effect from the surface SEI after the first cycle as can be seen in Fig. 4(b). This can be attributed to the surface film which prevents the electrolyte from being further oxidized. Therefore, the capacity loss in the full cell is mainly due to the SEI formation on the surface of graphite.

Conclusion

A simple polymer-assisted method to prepare self-substitution high voltage cathode $LiMn_{1.6}Ni_{0.4}O_4$ is reported. The cathode materials showed a stable capacity at a 4 C rate. Mn doping in the crystal structure helps stable the structure, and the carbon layer helps the structure stability and cycling stability. The stable electrode–electrolyte interface also helps prevent the further oxidation of electrolyte. The reduction of Mn ions is considered as one of the reasons for the degradation of the electrode due to Jahn–Teller effect which is associated with Mn^{3+}. Without the carbon layer protection, capacity faded quickly. A successful implementation of this cathode in full cell with graphite anodes confirms that the high voltage cathode is a promising candidate for lithium-ion batteries with high energy density.

References

[1] Liu, J., and Manthiram, A., 2009, "Understanding the Improved Electrochemical Performances of Fe-Substituted 5 V Spinel Cathode $LiMn_{1.5}Ni_{0.5}O_4$," J. Phys. Chem. C, **113**(33), pp. 15073–15079.

[2] Shin, D. W., Bridges, C. A., Huq, A., Paranthaman, M. P., and Manthiram, A., 2012, "Role of Cation Ordering and Surface Segregation in High-Voltage Spinel $LiMn_{1.5}Ni_{0.5-x}M_xO_4$ (M = Cr, Fe, and Ga) Cathodes for Lithium-Ion Batteries," Chem. Mater., **24**(19), pp. 3720–3731.

[3] Liu, J., and Manthiram, A., 2009, "Improved Electrochemical Performance of the 5 V Spinel Cathode $LiMn_{1.5}Ni_{0.42}Zn_{0.08}O_4$ by Surface Modification," J. Electrochem. Soc., **156**(1), pp. A66–A72.

[4] Yi, T.-F., Xie, Y., Zhu, Y.-R., Zhu, R.-S., and Ye, M.-F., 2012, "High Rate Micron-Sized Niobium-Doped $LiMn_{1.5}Ni_{0.5}O_4$ as Ultra High Power Positive-Electrode Material for Lithium-Ion Batteries," J. Power Sources, **211**, pp. 59–65.

[5] Arunkumar, T. A., and Manthiram, A., 2005, "Influence of Lattice Parameter Differences on the Electrochemical Performance of the 5 V Spinel $LiMn_{1.5-y}Ni_{0.5-z}M_{y+z}O_4$ (M = Li, Mg, Fe, Co, and Zn)," Electrochem. Solid-State Lett., **8**(8), pp. A403–A405.

[6] Kunduraci, M., and Amatucci, G. G., 2007, "Effect of Oxygen Non-Stoichiometry and Temperature on Cation Ordering in $LiMn_{2-x}Ni_xO_4$ ($0.50 \geq x \geq 0.36$) Spinels," J. Power Sources, **165**(1), pp. 359–367.

[7] Liu, H., Wang, J., Zhang, X., Zhou, D., Qi, X., Qiu, B., Fang, J., Kloepsch, R., Schumacher, G., Liu, Z., and Li, J., 2016, "Morphological Evolution of High-Voltage Spinel $LiNi_{0.5}Mn_{1.5}O_4$ Cathode Materials for Lithium-Ion Batteries: The Critical Effects of Surface Orientations and Particle Size," ACS Appl. Mater. Interfaces, **8**(7), pp. 4661–4675.

[8] Hwang, T., Lee, J. K., Mun, J., and Choi, W., 2016, "Surface-Modified Carbon Nanotube Coating on High-Voltage $LiNi_{0.5}Mn_{1.5}O_4$ Cathodes for Lithium Ion Batteries," J. Power Sources, **322**, pp. 40–48.

[9] Kumar, P. R., Madhusudhanrao, V., Nageswararao, B., Venkateswarlu, M., and Satyanarayana, N., 2016, "Enhanced Electrochemical Performance of Carbon-Coated $LiMPO_4$ (M = Co and Ni) Nanoparticles as Cathodes for High-Voltage Lithium-Ion Battery," J. Solid State Electrochem., **20**(7), pp. 1855–1863.

[10] Myung, S.-T., Komaba, S., Kumagai, N., Yashiro, H., Chung, H.-T., and Cho, T.-H., 2002, "Nano-Crystalline $LiNi_{0.5}Mn_{1.5}O_4$ Synthesized by Emulsion Drying Method," Electrochim. Acta, **47**(15), pp. 2543–2549.

[11] Xu, Y., Chen, G., Fu, E., Zhou, M., Dunwell, M., Fei, L., Deng, S., Andersen, P., Wang, Y., Jia, Q., and Luo, H., 2013, "Nickel Substituted $LiMn_2O_4$ Cathode With Durable High-Rate Capability for Li-Ion Batteries," RSC Adv., **3**(40), pp. 18441–18445.

[12] Rana, J., Glatthaar, S., Gesswein, H., Sharma, N., Binder, J. R., Chernikov, R., Schumacher, G., and Banhart, J., 2014, "Local Structural Changes in $LiMn_{1.5}Ni_{0.5}O_4$ Spinel Cathode Material for Lithium-Ion Batteries," J. Power Sources, **255**, pp. 439–449.

[13] Mukai, K., Ikedo, Y., Kamazawa, K., Brewer, J. H., Ansaldo, E. J., Chow, K. H., Mansson, M., and Sugiyama, J., 2013, "The Gradient Distribution of Ni Ions in Cation-Disordered $Li[Ni_{1/2}Mn_{3/2}]O_4$ Clarified by Muon-Spin Rotation and Relaxation (μSR)," RSC Adv., **3**(29), pp. 11634–11639.

[14] Chemelewski, K. R., and Manthiram, A., 2013, "Origin of Site Disorder and Oxygen Nonstoichiometry in $LiMn_{1.5}Ni_{0.5-x}M_xO_4$ (M = Cu and Zn) Cathodes With Divalent Dopant Ions," J. Phys. Chem. C, **117**(24), pp. 12465–12471.

[15] Manthiram, A., Chemelewski, K., and Lee, E.-S., 2014, "A Perspective on the High-Voltage $LiMn_{1.5}Ni_{0.5}O_4$ Spinel Cathode for Lithium-Ion Batteries," Energy Environ. Sci., **7**(4), pp. 1339–1350.

[16] Samarasingha, P. B., Andersen, N. H., Sørby, M. H., Kumar, S., Nilsen, O., and Fjellvåg, H., 2016, "Neutron Diffraction and Raman Analysis of $LiMn_{1.5}Ni_{0.5}O_4$ Spinel Type Oxides for Use as Lithium Ion Battery Cathode and Their Capacity Enhancements," Solid State Ionics, **284**, pp. 28–36.

[17] Yamada, A., 1996, "Lattice Instability in $Li(Li_xMn_{2-x})O4$," J. Solid State Chem., **122**(1), pp. 160–165.